

Efficiency Enhancement of Feedforward Amplifiers by Employing a Negative Group-Delay Circuit

Heungjae Choi, *Student Member, IEEE*, Yongchae Jeong, *Member, IEEE*, Chul Dong Kim, *Member, IEEE*, and J. Stevenson Kenney, *Fellow, IEEE*

Abstract—We will demonstrate an alternative topology for the feedforward amplifier. This amplifier does not use a delay element, thus providing an efficiency enhancement and a size reduction by employing a distributed-element negative group-delay circuit. The insertion loss of the delay element in the conventional feedforward amplifier seriously degrades the efficiency. Usually, a high-power coaxial cable or a delay-line filter is utilized for a low loss, but the insertion loss, cost, and size of the delay element still act as a bottleneck. The proposed negative group-delay circuit removes the necessity of the delay element required for a broadband signal suppression loop. With the fabricated two-stage distributed-element negative group-delay circuit with 30 MHz of bandwidth and -9 ns of group delay for a wideband code-division multiple-access downlink band, the feedforward amplifier with the proposed topology experimentally achieved 19.4% power-added efficiency and -53.2 -dBc adjacent channel leakage ratio with 44-dBm average output power.

Index Terms—Distributed element, efficiency enhancement, feedforward amplifier, negative group-delay circuit, transmission-line resonator, wideband code-division multiple access (WCDMA).

I. INTRODUCTION

SINCE ITS first introduction by Black [1], [2] and the experiment by Seidel [3], the feedforward amplifier system has played a leading role for linear transmitters, especially in the base-station applications used in a modern wireless communication environment. In addition to the feedforward method, there are various linearization techniques, including analog predistortion, digital predistortion, and by direct or indirect feedback, such as in a polar method or in a Cartesian loop [4]. Nevertheless, the feedforward technique has become a preferred technique and is well known for its broad bandwidth capability, good linearization performance, and stable operation. This is due to the fact that it operates by the utilization of forward loops.

Extensive research on the analysis and design of the feedforward amplifier system has been done. Potheary [5], Kenington

[6], and other researchers [7]–[9] have analyzed the effects of amplitude, out-of-phase, and delay mismatches on the suppression and efficiency performance of these amplifiers. Andrenko *et al.* [10] and Larose and Ghannouchi [11], [12] have proposed efficiency optimizations of the feedforward amplifier. As a system model, Rummery and Branner [13] have proposed a first-order closed-form equation for the feedforward design constraints and sensitivity analysis. Jeong *et al.* [14] proposed an equal group-delay signal canceller to improve the inherent bandwidth limitation of the signal subtraction circuit by using an in-phase combiner/divider with a 180° phase difference. Hau *et al.* [15] proposed a phase equalizer to reduce the nonlinear phase imbalances within the suppression loops. Braithwaite [16] described a novel pilot generation and detection system for an adaptive feedforward amplifier. Choi *et al.* [17] expanded the feedforward amplifier to a dual-band operation and modified a cross-cancellation technique for the feedforward amplifier, used as efficiency and linearity enhancement for a balanced power amplifier [18].

Major sources of efficiency degradation for the feedforward amplifier are found in the error power amplifier (EPA) employed at the distortion suppression loop and passive components connected at the output of the main power amplifier (MPA), especially the insertion loss of a delay element. The delay element is unavoidable and essential to the broadband signal suppression loop design, as long as there is a propagation time for the EPA and the accompanying adjustable devices required for loop balancing.

Recently, interesting experimental validation on the negative group delay (NGD) concept has been reported, and its electronic circuit application has been proposed. The NGD concept is quite intriguing, and sometimes confusing, in that typical materials under normal conditions do not usually behave in a manner consistent with the observed behaviors. In a specific frequency band of an anomalous dispersion, the group velocity is observed to be greater than that of c , which is the speed of light in vacuum, or even a negative value. This phenomenon was defined as the superluminal group velocity [19], [20]. Researchers have been trying to find an application of NGD or the superluminal effect to various electronic circuits [21]–[24]. In [25]–[27], various applications of the NGD circuits with an active topology have been proposed. In [28], a trial to design a passive NGD circuit for the feedforward power amplifier application was reported. However, the previous work was not suitable for a commercial linear power amplifier (LPA) system amplifying broadband modulated signals, such as wideband code-division multiple-access (WCDMA) signals in which the signal bandwidth is roughly 5 MHz. This is due to a narrow signal bandwidth

Manuscript received October 24, 2009; revised February 07, 2010. First published April 22, 2010; current version published May 12, 2010.

H. Choi and Y. Jeong are with the Department of Information and Communication Engineering, Chonbuk National University, Jeonju 561-756, Korea (e-mail: streetpoet@jbnu.ac.kr; ycjeong@jbnu.ac.kr).

C. D. Kim is with Sewon Teletech Inc., Kyungki 431-084, Korea (e-mail: chuldokim@sewon-teletech.co.kr).

J. S. Kenney is with the School of Electrical and Computer Engineering, Georgia Institute of Technology, Atlanta, GA 30332 USA (e-mail: jskenney@ece.gatech.edu).

Color versions of one or more of the figures in this paper are available online at <http://ieeexplore.ieee.org>.

Digital Object Identifier 10.1109/TMTT.2010.2045576

(2 MHz of two-tone spacing), poor input/output reflection coefficients, design inaccuracy induced by the limited availability of lumped elements, and the fact that there was no intuitive general NGD circuit design equation. Considering the intermodulation distortion (IMD) signal, the bandwidth requirements would be much harder to satisfy in practical applications.

This paper presents a novel topology of the feedforward amplifier without a delay element by employing a distributed-element (DE) NGD circuit. The major benefit that can be achieved with the proposed topology is an efficiency enhancement accomplished by eliminating the delay element at the output of the MPA, which is one of the major sources of efficiency degradation, without affecting the linearization performance.

This paper is organized as follows. Section II describes the proposed novel feedforward structure. A reinvestigation of the conventional analysis of the loop suppression with respect to the amplitude, out-of-phase, and especially group-delay mismatch in nanoseconds is discussed for intuitive understanding, which has not been presented in previous works. Also, the major sources of the efficiency degradation for the power-amplifier linearization technique and the solution for the efficiency enhancement are discussed. In Section III, the DE NGD circuit is presented along with the expected advantages when applied to the proposed system. Experimental verification results and a table of measurement results compared with the previous works are demonstrated in Section IV, which is followed by the conclusion in Section V.

II. NGD FEEDFORWARD ARCHITECTURES AND ANALYSIS

A. Feedforward Amplifier Without Delay Element

Since the feedforward amplifier is a well-known architecture, a detailed description will not be given in this paper. Fig. 1 illustrates the two types of feedforward amplifiers employing the NGD circuit proposed in this paper. The NGD circuit and a bandpass filter (BPF) are added in the conventional feedforward structure. A BPF is used to avoid any unwanted oscillation in forward loops. In Fig. 1(a), the NGD circuit is placed in the EPA path and counterbalances the group-delay time experienced by the EPA path including the vector modulator, the EPA, and other coupling devices. In that way, the delay element (*DELAY 2*) at the output of the MPA can be eliminated. In this case, the eliminated delay element gives us an efficiency enhancement for the feedforward amplifier without affecting the carrier suppression loop. In Fig. 1(b), the NGD circuit is inserted into the common path of the two loops.

Therefore, the delay elements from the carrier suppression loop (*DELAY 1*) as well as the IMD suppression loop (*DELAY 2*) can be reduced or eliminated. If the group delays of the MPA and the EPA path are same, the complete elimination of the two delay elements is possible, therefore enhancing the efficiency and minimizing the total size of the feedforward system. Even though the delay element is eliminated, additional power-consuming circuits must be added to the NGD circuit. However, an important difference is that the newly adopted NGD circuit consumes a very small dc power component as compared with the power lost by the delay elements when placed at the output of the MPA. Also, the NGD circuit is able to be integrated in

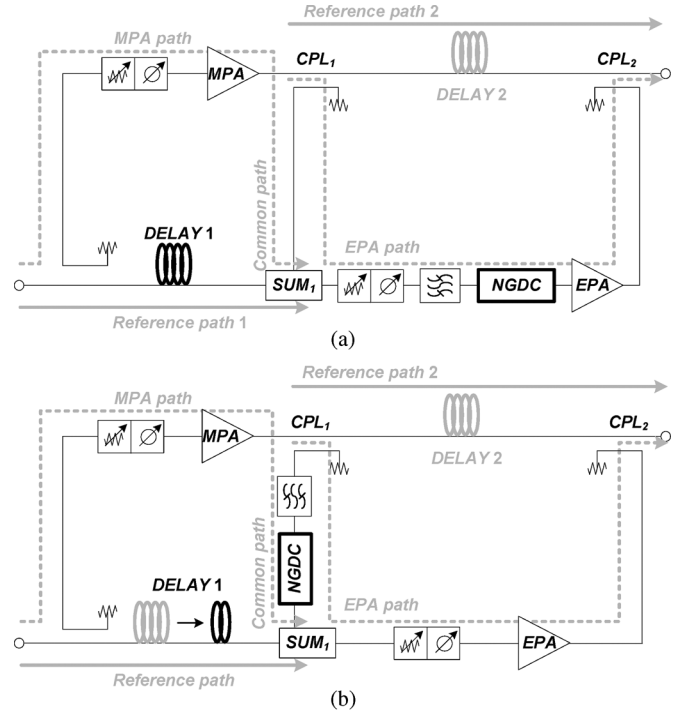


Fig. 1. Proposed novel feedforward amplifier topologies with NGD circuit employed at: (a) EPA path and (b) common path.

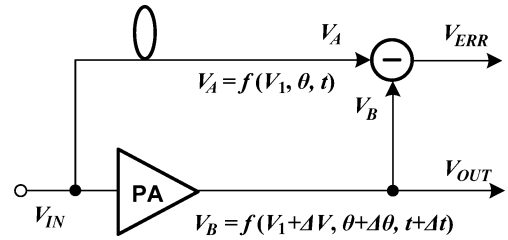


Fig. 2. Simple signal-suppression loop model.

the EPA module, while the delay elements are typically composed of bulky delay-line filters or high-power coaxial cables with the inevitable size, weight, and cost penalty. In this work, the topology of Fig. 1(b) is chosen.

B. Signal-Suppression Loop Analysis for Group-Delay Mismatch

Fig. 2 shows the simple signal-suppression loop model representing the amplitude, out-of-phase, and group-delay mismatches. A portion of the input signal (V_{IN}) is coupled into the delay path as a reference signal (V_A). The remaining portion of the V_{IN} is amplified by the PA resulting in the amplified carrier with IMD components. A portion of the output of PA (V_B) is then coupled into the subtraction circuit, which is then destructively combined with the V_A , generating an error signal (V_{ERR}) that theoretically does not include any carrier components.

1) *Amplitude and Out-of-Phase Mismatch:* When the reference signal of a sinusoidal waveform having an amplitude (V_1) and a phase (θ) is combined with the signal that includes the amplitude mismatch factor (ΔV) and the out-of-phase mismatch

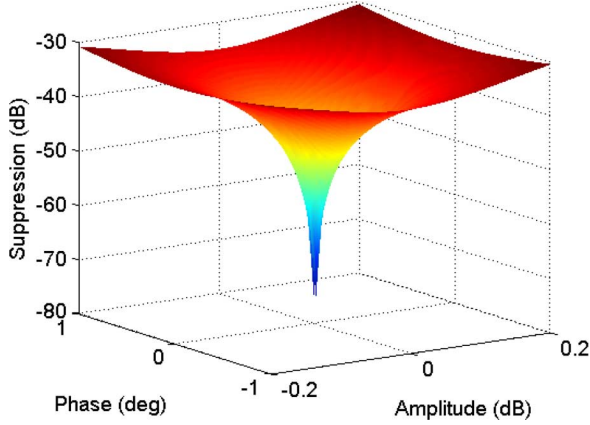


Fig. 3. Loop suppression expressed as a function of amplitude and phase mismatch.

factor ($\Delta\theta$), the resultant carrier-suppressed signal can be represented as a ratio of the average power of V_{ERR} to V_A [5] as

$$S(\text{dB}) = 10 \log \left[1 + \left(\frac{V_1 + \Delta V}{V_1} \right)^2 - 2 \left(\frac{V_1 + \Delta V}{V_1} \right) \cdot \cos(\Delta\theta) \right]. \quad (1)$$

Fig. 3 shows the calculated loop suppression performance expressed as a function of an amplitude mismatch of ± 0.2 dB and an out-of-phase mismatch of $\pm 1^\circ$. From the figure, this mismatching range leads to a loop suppression of about -30 dB, where the group-delay (GD) mismatch is assumed to be zero in this analysis.

2) *GD Mismatch*: The GD mismatch (Δt) between the paths is critical for broadband signal suppression. For our analysis, we assumed a unit amplitude ($V_1 = 1$) and a perfectly matched amplitude and out-of-phase condition ($\Delta V = \Delta\theta = 0$). V_{ERR} can be expressed as follows:

$$\begin{aligned} V_{ERR} &= V_A + V_B \\ &= \cos(\omega_0 t + \theta) \cos(\omega_0(t + \Delta t) + \theta + 180^\circ) \\ &= \cos(\omega_0 t + \theta) (1 - \cos(\omega_0 \Delta t)) \\ &\quad + \sin(\omega_0 t + \theta) \sin(\omega_0 \Delta t) \end{aligned} \quad (2)$$

where ω_0 is an angular frequency.

To calculate the average power over one period, $|V_{ERR}|^2$ can be obtained by using (2) to yield

$$\begin{aligned} |V_{ERR}|^2 &= \left| \frac{(1 - \cos \omega_0 \Delta t)^2 + (1 - \cos \omega_0 \Delta t)^2 \cos 2(\omega_0 t + \theta)}{2} \right. \\ &\quad + \frac{\sin^2(\omega_0 \Delta t) + \sin^2(\omega_0 \Delta t) \sin^2(\omega_0 t + \theta)}{2} \\ &\quad \left. + \sin 2(\omega_0 t + \theta) (1 - \cos \omega_0 \Delta t) (\sin \omega_0 \Delta t) \right|. \end{aligned} \quad (3)$$

By taking an integral of (3) over an arbitrary period T_0 , the average power of V_{ERR} is given by

$$P_{ERR,avg} = 1 - \cos \omega_0 \Delta t. \quad (4)$$

Since the ratio of (4) to the average power of the V_A ($P_A = 1/2$) is defined as the loop suppression, we can express the loop

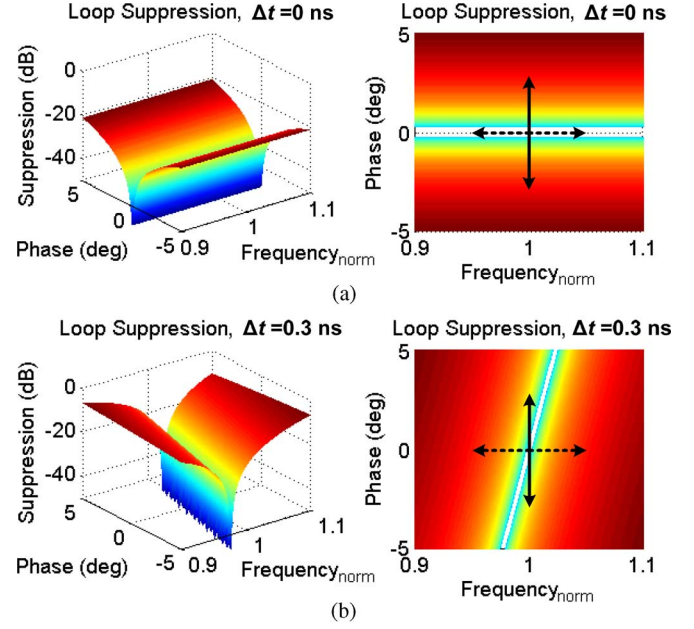


Fig. 4. Loop-suppression performance expressed as a function of phase and GD mismatch when: (a) $\Delta t = 0$ ns and (b) $\Delta t = 0.3$ ns (at a fixed amplitude mismatch of 0.01 dB).

suppression in a decibel scale for a time-mismatching condition as shown by

$$S_{\Delta t} = 10 \log (1 - (\cos(\omega_0 \Delta t)) \cdot (1 - f/f_0)) + 3 \quad (5)$$

where the term $1 - f/f_0$ is inserted to derive the equation with respect to the normalized frequency ($\text{Frequency}_{\text{norm}}$ in Fig. 4) when f_0 represents the center frequency.

Finally, from (1) and (5), we can derive the loop-suppression equation considering the amplitude, out-of-phase, and delay mismatches to be represented as a function of time (Δt) as

$$\begin{aligned} S_{\text{total}} &= 10 \log \left[1 + \left(\frac{V_1 + \Delta V}{V_1} \right)^2 - 2 \left(\frac{V_1 + \Delta V}{V_1} \right) \right. \\ &\quad \left. \cdot \cos(\omega_0 \Delta t) \left(1 - \frac{f}{f_0} \right) \right]. \end{aligned} \quad (6)$$

Fig. 4 shows the loop-suppression performance with and without the presence of a delay mismatch for 0.01 dB of fixed amplitude mismatch. In the case there is no delay mismatch, as shown in Fig. 4(a), the loop-suppression performance is only limited by the out-of-phase mismatch, not by the normalized frequency, as the dotted arrow direction designates. However, in the presence of 0.3 ns of delay mismatch, the amount of the loop-suppression performance is limited both by the phase (solid line) and the normalized frequency (dotted line), as shown in Fig. 4(b).

Fig. 5 shows the calculated and the simulated loop-suppression performance, with respect to the normalized frequency, for a different delay mismatch when there is 0.01 dB of amplitude mismatch with no phase mismatch. The mathematical estimation closely agrees with the circuit simulation by using Agilent's Advanced Design System (ADS) 2009. In case of 0.3 ns

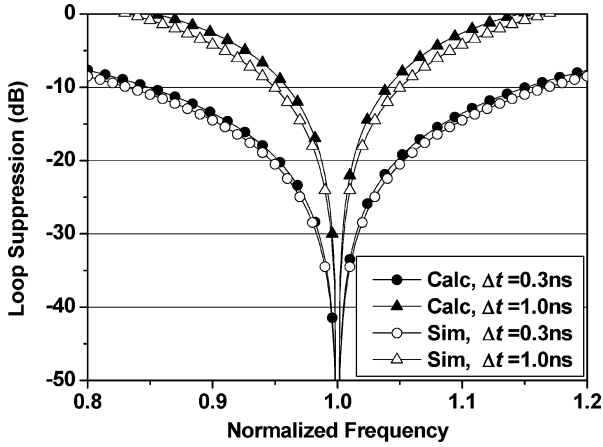


Fig. 5. Calculated and simulated loop-suppression performance expressed as a function of normalized frequency for different time-mismatching values.

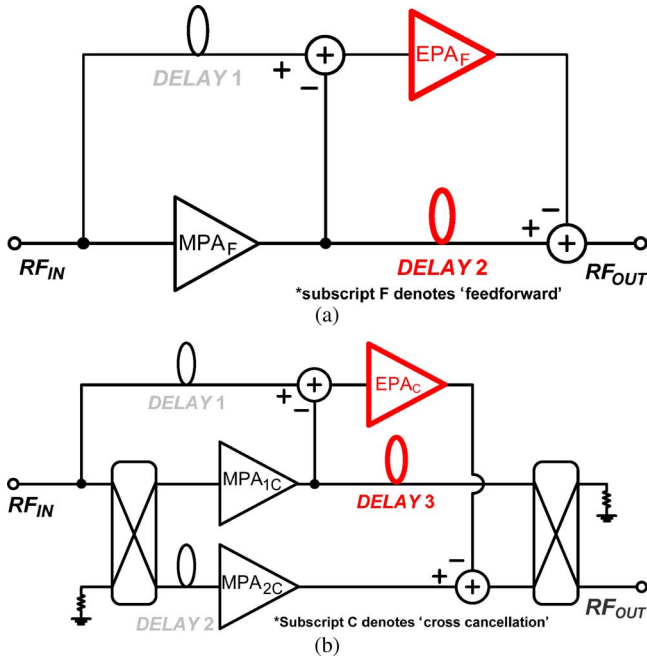


Fig. 6. Block diagrams of: (a) typical feedforward power amplifier and (b) cross-cancellation technique.

of GD mismatching, we can expect that the fractional bandwidth of 20-dB cancellation will be 5.2%. When the mismatch is 1.0 ns, the bandwidth is considerably decreased to 1.6%, which is nearly 30% of the bandwidth for 0.3-ns mismatch.

C. Efficiency Degradation of Linear Amplifier System

As already discussed in the previous sections, the major sources of efficiency degradation for the feedforward amplifier are the dc power consumption of the EPA employed at the distortion suppression loop and the insertion loss of the passive components (*DELAY 2*) connected at the output of the MPA, as shown in Fig. 6(a). The other example, Fig. 6(b), shows the power amplifier linearized by the cross-cancellation technique [18]. In this case, there is also a delay element (*DELAY 3*) at the output of MPA_{1C} to compensate for the group delay due to EPA_C .

By carefully defining the class of operation, the power capacity ratio of the MPA to EPA, and the desired amount of IMD suppression, we can minimize the dc power consumption and optimize efficiency [12]. However, the delay element is unavoidable and is essential to achieve broadband signal suppression as long as there is a propagation time for the EPA and the accompanying adjustable devices, such as the vector modulators required for loop balancing. By minimizing or eliminating the delay of the EPA path, the insertion loss of the delay element can be minimized. As a result, the desired efficiency-enhanced feedforward power amplifier can be realized.

After the introduction of the NGD, a zero-propagation-time system that combines the NGD circuit and the conventional delay circuit has become an actual and achievable characteristic for RF and microwave circuits. The physical nature, causality issues, and electric circuit approach that apply to the NGD have been already analyzed and proved with experimental observations [19]–[30]. By adopting the NGD concept, the delay element known to be the major efficiency-degrading component required for the signal-suppression loop can be totally eliminated, resulting in the efficiency enhancement of the PA linearization techniques.

III. CIRCUIT IMPLEMENTATIONS

A. DE NGD Circuit

In a medium of refractive index $n(\omega)$, the dispersion relation can be written

$$k = \frac{\omega n}{c} \quad (7)$$

where κ is the wave number. The group velocity (v_g), which means the speed of the envelope signal, is then given by

$$v_g = \frac{c}{n + \omega \text{Re}[dn/d\omega]}. \quad (8)$$

From (9) and (10), it can be inferred that, if the refractive index decreases rapidly with regard to the frequency, the group velocity and the group delay can become negative, and this event does happen near an absorption line or signal attenuation condition, where “anomalous” wave propagation effects can occur [20]. Typically, in RF circuit design that is based on the dielectric laminate, we cannot control the refractive index of the given material. Therefore, we are only able to obtain the NGD through the signal attenuation condition, which can be easily compensated with the small-signal gain amplifier without reducing the amount of NGD.

The design equations for the transmission-type series-parallel (SP) and shunt-series (SS) NGD circuit have already been derived in [29]. A reflective circuit, however, is useful to improve the input/output reflection characteristics of RF circuits, such as a variable phase shifter and a variable attenuator using a 3-dB hybrid.

Fig. 7 shows the lumped-element (LE) prototype circuits of the reflective parallel (RP) and reflective series (RS) NGD circuit [30]. The magnitude and phase of the reflection coefficient for the RP network (Γ_{RP}) can be obtained by using the input

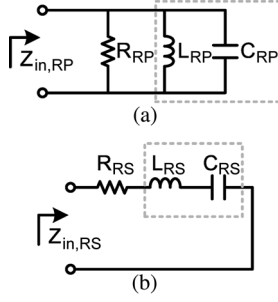


Fig. 7. LE prototype NGD circuits. (a) Reflective parallel structure. (b) Reflective series structure.

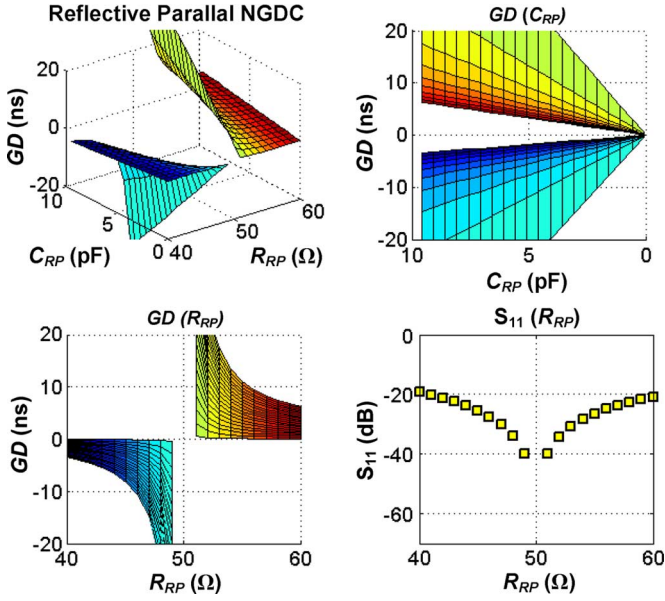


Fig. 8. Calculated GD and reflection loss according to R_{RP} and C_{RP} , from [30].

impedance of the RP network. Then, the GD and the reflection loss can be represented by

$$GD_{RP}|_{\omega=\omega_0} = -\left. \frac{d\phi_{in,RP}}{d\omega} \right|_{\omega=\omega_0} = \frac{4R_{RP}^2 Y_0 C_{RP}}{(R_{RP} Y_0)^2 - 1} \quad (9)$$

$$\Gamma_{RP}|_{\omega=\omega_0} = \frac{1 - R_{RP} Y_0}{1 + R_{RP} Y_0} \quad (10)$$

by assuming a resonance condition for the desired operating frequency. The GD is a function of the capacitance (C_{RP}) and the resistance (R_{RP}).

For good understanding and design, (9) and (10) were calculated using a MATLAB program according to C_{RP} and R_{RP} , especially for $40 \Omega < R_{RP} < 60 \Omega$ and $0 \text{ pF} < C_{RP} < 10 \text{ pF}$ as in Fig. 8. The amount of NGD is proportional to R_{RP} and C_{RP} , provided that R_{RP} is smaller than 50Ω . In case of $R_{RP} > 50 \Omega$, the NGD circuit abruptly cause a positive GD. From the subplot of Fig. 8 illustrating the reflection loss with respect to R_{RP} , it can be inferred that more NGD induces more signal attenuation, delivering a tradeoff to the designer.

One major difficulty of the LE circuit is the feasibility of the designed component values. In a microwave circuit design,

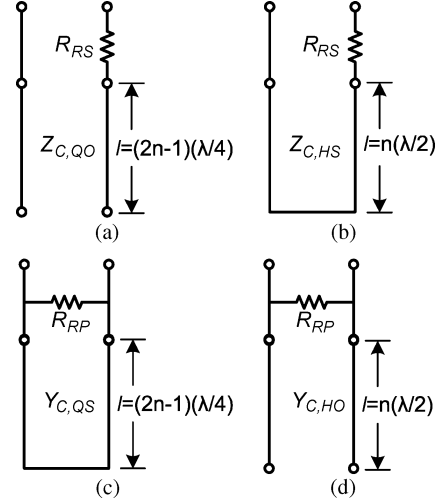


Fig. 9. Four types of DE NGD circuits: (a) quarter-wavelength open; (b) half-wavelength short; (c) quarter-wavelength short; (d) half-wavelength open circuit, from [30].

a specific length of open or short terminated transmission line is often used as a resonator, called a transmission-line resonator (TLR) [31]. Fig. 9 shows the four types of DE NGD circuits converted from the LE prototype circuit. It is noted that Fig. 9(a) and (c) have an odd multiple of the quarter-wavelength, and Fig. 9(b) and (d) have a multiple of the half-wavelength, with $n = 1$ being chosen for a small size. The RP network in Fig. 7(a) can be converted either into the quarter-wavelength short circuit (QS) of Fig. 9(a) or the half-wavelength open circuit (HO) of Fig. 9(b). The RS network in Fig. 7(b) can be converted either into the quarter-wavelength open circuit (QO) of Fig. 9(c) or the half-wavelength short circuit (HS) of Fig. 9(d). The characteristic impedance and admittance for the four types of TLR can be derived as follows, respectively:

$$Y_{C,QS} = \frac{4\omega_0 C_{RP}}{\pi} \quad (11)$$

$$Y_{C,HO} = \frac{2\omega_0 C_{RP}}{\pi} \quad (12)$$

$$Z_{C,HS} = \frac{2\omega_0 L_{RS}}{\pi} \quad (13)$$

$$Z_{C,QO} = \frac{4\omega_0 L_{RS}}{\pi} \quad (14)$$

An example to show the validity of a prototype RP LE NGD circuit and its equivalent DE circuit were simulated. By using (9) and Fig. 7, we calculated that $R_{RP} = 47.5 \Omega$, $C_{RP} = 5.0 \text{ pF}$, and $L_{RP} = 1.107 \text{ nH}$ to obtain a -9-ns GD, and the estimated reflection loss was -31.82 dB derived from (10) at the center frequency of 2.14 GHz . Then, the LE circuit was converted into the TLR using (11), and the calculated characteristic impedance for the QS was 60.16Ω . As shown in Fig. 10, since there are a number of combinations for LC resonating pairs, C_{RP} should be carefully chosen so that the characteristic impedance of TLR should not exceed the practical range. Larger amounts of NGD value beyond 10 ns involve the bandwidth limitation as well as the higher insertion loss. As a prototype, a microstrip 3-dB branchline coupler is designed as a 90° hybrid. To reduce the

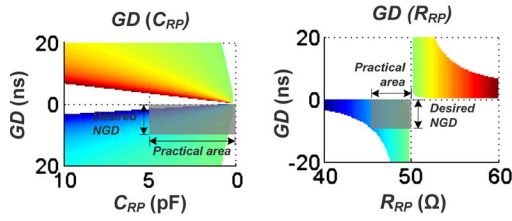
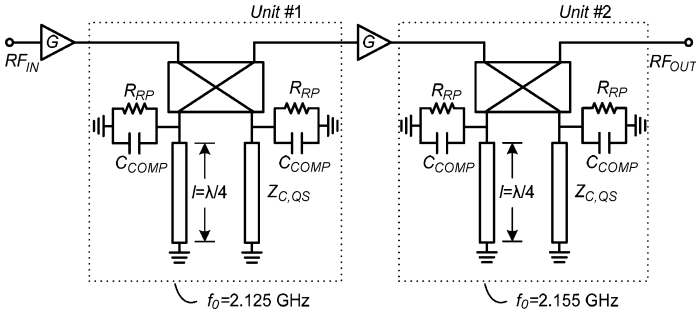

 Fig. 10. Practical range for NGD circuit design according to R_{RP} and C_{RP} .


Fig. 11. Circuit diagram of two-stage reflection-type NGD circuit, from [30].

circuit size, a commercial, low-profile, and miniature 3-dB hybrid coupler with a surface-mount package can be used.

For an experimental verification, we set as our goal the design of a two-stage reflective DE NGD circuit with -9 ns of total GD, close to 0-dB insertion loss, and a 30-MHz bandwidth centered on the WCDMA downlink band (2.125 ~ 2.155 GHz). This NGD value is chosen for the compensation of the signal transmission time due to the circuits in the EPA path in a feedforward technique. The proposed circuit would be constructed of 90° hybrids and two DE NGD circuit units (#1 and #2), of which the center frequencies were 2.125 and 2.155 GHz, respectively, as shown in Fig. 11. By connecting the two units in a cascade, we hoped to obtain a flat GD and transmission response. The insertion loss of the NGD circuit itself could be compensated by a general-purpose small-signal amplifier as shown in Fig. 11. A compensation capacitor (C_{COMP}) would be connected in parallel to the R_{RP} to compensate for the minute parasitic inductance of a chip resistor so that R_{RP} would not have any reactive impedance. Total size of the fabricated two-stage DE NGD circuit is $180 \times 90 \text{ mm}^2$.

Fig. 12 shows the simulation and measurement results of the two-stage DE NGD circuit. One notable advantage of the proposed topology is that the same magnitude and GD response can be obtained when the position of the gain amplifier is changed. In other words, the first gain amplifier (G) can be moved to the output of the second NGD circuit (Unit #2) according to the input power level. In that way, we can avoid the potential nonlinear distortion generation in the NGD module. The measured results of Fig. 12(a) agree well with the simulation results, where the measured GD and the insertion loss were -9 ± 0.25 ns and -0.21 ± 0.06 dB in the operating frequency, respectively. The small amount of GD and magnitude error are due to the connecting elements and the gain of the small-signal amplifier.

Fig. 12(b) represents the phase jump observed in the NGD region. In the NGD region, the slope of the phase is observed to

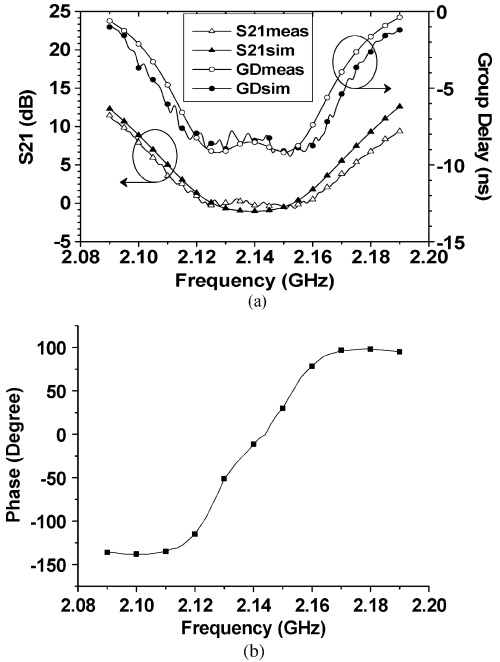


Fig. 12. Two-stage reflection-type NGD circuit. (a) Simulated and measured GD and insertion loss. (b) Measured phase response.

be positive, implying that the group velocity is negative. The negative group velocity can be translated as the direction of envelope propagation is opposite to the direction of the signal propagation. This inverted phase slope can be used to cancel out or control the negative phase slope (or positive GD) of the conventional circuit, consequently achieving zero phase slope (and, therefore, smaller or even zero GD). In the case that a larger negative GD would be necessary, a designer should make a tradeoff between the GD and the bandwidth. With regard to the additional dc power consumption in the NGD circuit, each small-signal amplifier consists of two ERA-5SM Mini-Circuits and consumes approximately 1 W. This dc power consumption is a relatively small amount when compared with the RF power loss in the *DELAY 2* of Fig. 2.

IV. EXPERIMENTAL RESULTS

The proposed feedforward amplifier was fabricated with a STA0821-3940MM-MS, 120-W PEP commercial power amplifier manufactured by Sewon Teletech Inc. with all of the options turned off, including the digital predistortion and the automatic power shutdown. This MPA could operate up to 49.18 dBm of the output power (laboratory measurement) with 54.8 dB of gain at 28 V. It had 38.3% of power-added efficiency (PAE) at peak power. The linearity specification for the base-station amplifier is -45 dBc for 5 MHz of frequency offset. The adjacent channel leakage ratio (ACLR) level of the MPA without the feedforward system was -33 dBc at an average output power of 44 dBm. Then, the power level of the nonlinear portion of the output signal is 11 dBm. If we select a 10-dB coupling ratio for an error injection coupler [CPL_2 shown in Fig. 1(b)], the EPA should be linear at an average output power of 21 dBm. In this work, the peak output power of the EPA is 41 dBm.

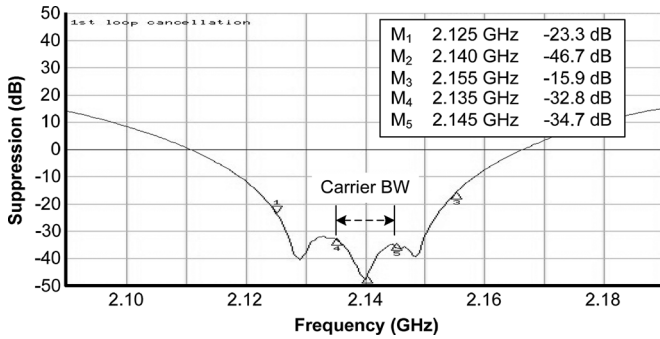


Fig. 13. Measured carrier suppression-loop characteristic.

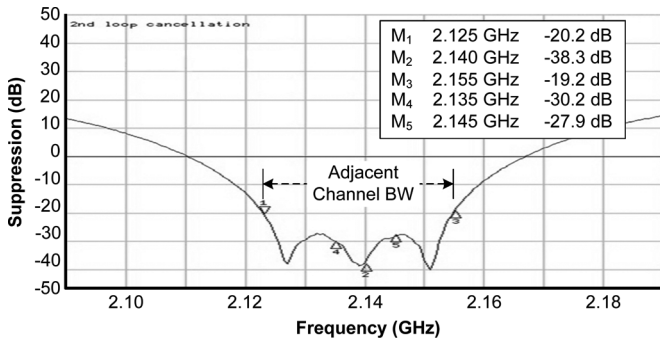


Fig. 14. Measured IMD suppression-loop characteristic.

Due to the frequency response of the employed NGD circuit, which amplified the unwanted out-of-band noise, the two-stage quarter-wavelength coupled-line BPF was designed with a microstrip line and integrated in front of the NGD circuit to avoid possible instabilities. The addition of narrowband BPF increases the total GD of the EPA path by 2.5 ns, and this factor has already been considered in the design of the NGD circuit in the previous section.

Figs. 13 and 14 show the measured suppression characteristics of the carrier suppression loop and the IMD suppression loop, respectively. For the carrier bandwidth of the two-carrier WCDMA signal, at about 10 MHz, at least -32.8 dB of carrier suppression could be achieved. When we took the adjacent channel bandwidth into account for the IMD suppression loop, over 19.2 dB of ACLR improvement was expected to be achieved for 30 MHz.

Fig. 15 shows the measured spectrum of the fabricated feedforward amplifier for a two-carrier WCDMA signal at an average output power of 43 dBm. The ACLR improvement was almost 20 dB from -36.6 dBc (Without_Cancel) to -56.6 dBc (With_Cancel) at a 5-MHz offset.

Fig. 16 illustrates the measured ACLR before and after linearization for an 8-dB output dynamic range. Optimized for 43 dBm of the output power, the fabricated system achieved at least -53 dBc of the ACLR at a 5-MHz offset for an output power of 37–44 dBm.

The measured ACLR and PAE performance with respect to the average output power is presented in Fig. 17. At an output power of 43 dBm, the ACLR was -56.6 dBc and PAE was 17%. At an average output power of 44 dBm, the measured ACLR and PAE (or drain efficiency) were -53.2 dBc and 19.4% (or

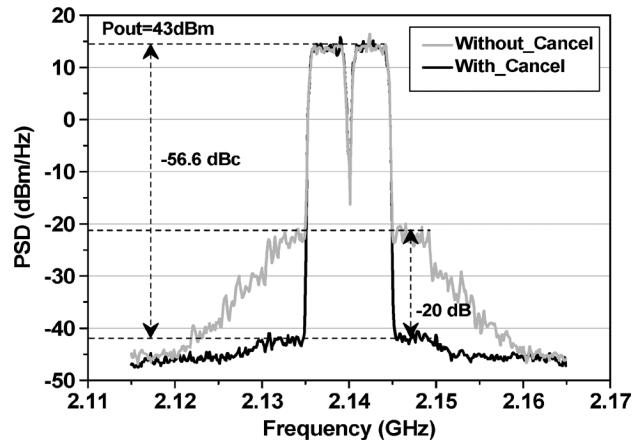


Fig. 15. Measured two-carrier WCDMA spectra before (Without_Cancel) and after (With_Cancel) linearization at an average output power of 43 dBm.

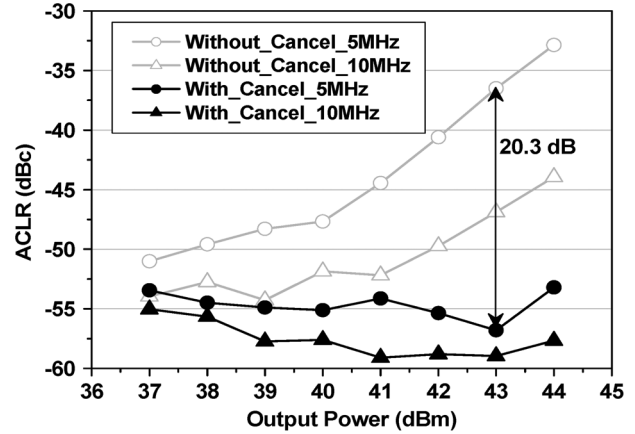


Fig. 16. Measured ACLR at 5- and 10-MHz offset of the proposed feedforward amplifier.

19.5%), respectively. This included the additional power consumption of the NGD circuit. For the MPA, the ACLR and PAE were -53.2 dBc and 5.1%, respectively, at an average output power of 36 dBm. For the same ACLR level with and without the proposed feedforward topology, the PAE of the system increased from 5.1% to 19.4%. Also, considering -53.2 dBc of ACLR as a reference, the available output power for the MPA increased from 36 to 44 dBm.

In detail, the GD difference between the conventional and the proposed structure is summarized in Table I. DELAY1 and DELAY2 denote the delay elements at reference path 1 (carrier suppression loop) and reference path 2 (IMD suppression loop) shown in Fig. 1, respectively. A value of 8.9 ns of the total compensating GD required at the output of the MPA is reduced to 1.2 ns, which is 13.5% of the initial value. This value is the minimum experimentally achievable GD in a feedforward technique for the laboratory experiment, which is generated by the signal coupling and the error injecting coupler with the minimum connecting element.

Also, DELAY1 is reduced from 11.6 to 4.1 ns. The measured results and the performance comparisons among feedforward amplifiers are summarized in Table II. Systems using a two-tone test signal can easily obtain a relatively high efficiency due to

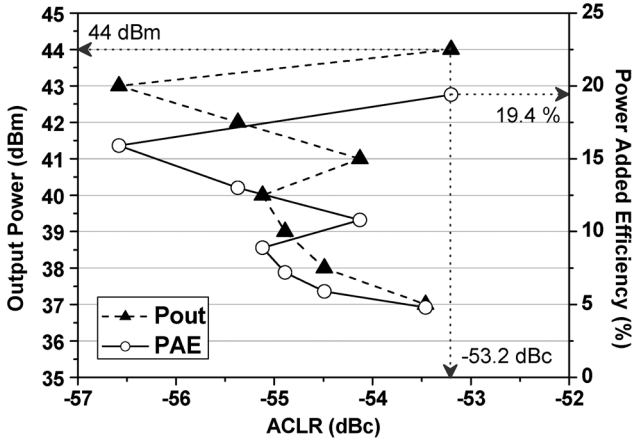


Fig. 17. Measured ACLR and PAE performance with respect to the average output power.

TABLE I
GD COMPARISON

	DELAY1 (ns)	DELAY2 (ns)
Conventional	11.6	8.9
This work	4.1	1.2

TABLE II
MEASUREMENT SUMMARY AND PERFORMANCE COMPARISON AMONG FEEDFORWARD AMPLIFIERS

	Frequency (GHz)	Pout (dBm)	Test Signal	Signal BW (MHz)	Linearity (dBc)	Drain Efficiency (%)
[11]	1.97	46.6	CDMA	3.75	-52	7
[28]	0.56	41	2-tone	2	-65	12
[32]	2.14	46.5	WCDMA	10	-55	13.6
[33]	2.14	26	2-tone	-	-	12
[34]	0.22	40	2-tone	0.05	-35	27
[35]	0.22	40	2-tone	0.05	-32	33
[36]	2.12	45.6	WCDMA	-	< -50	10
This work	2.14	44	WCDMA	10	-53	19.5

the low peak-to-average power ratio (PAPR), since the amplifier can be driven into a near-saturation level. However, in the case of transmitting a broadband modulated signal, higher efficiency is a difficult goal to achieve due to the high PAPR of the signal. The 19.5% of drain efficiency is the best result achieved with the feedforward amplifier at the time of this writing, according to the authors' best knowledge. This noticeable efficiency improvement is achieved by totally eliminating the delay element at the output of the MPA. If the output power of a given MPA is higher than what was used in this study, a few kilowatts, for example, then the efficiency enhancement will be much more evident since the effect of additional dc power consumption due to the small-signal amplifier in the NGD circuit will be negligible when compared with the power consumption of delay elements.

Fig. 18 shows the output spectra when a four-carrier WCDMA signal was applied to the proposed system. As observed in Fig. 14, in spite of the fact that the employed NGD circuit had 30 MHz of bandwidth, we could still obtain

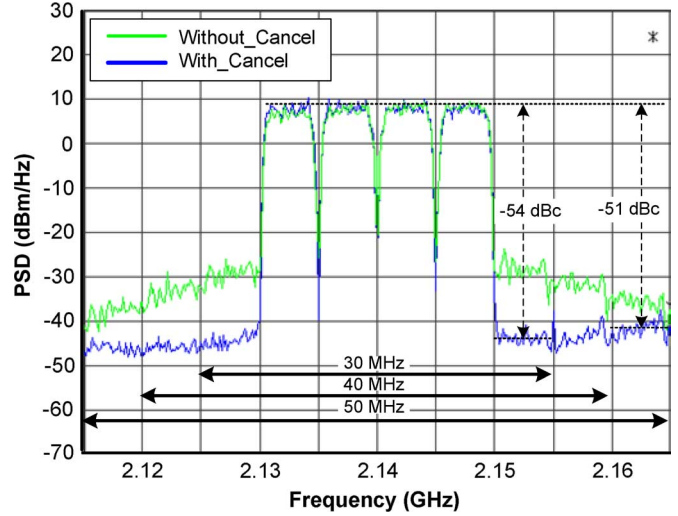


Fig. 18. Measured four-carrier WCDMA spectra before (Without_Cancel) and after (With_Cancel) linearization.

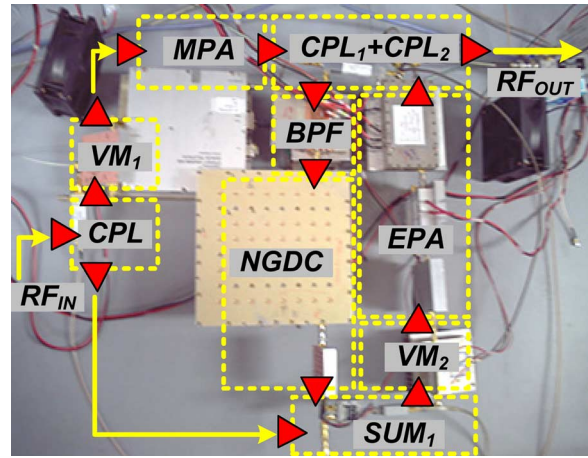


Fig. 19. Photograph of the proposed feedforward topology (VM₁ and VM₂ in the photograph refers to the vector modulator).

a linearization effect beyond the 30-MHz bandwidth. For a 40-MHz bandwidth, the measured ACLR at a 10-MHz offset is nearly -50 dBc, which still satisfies the minimum WCDMA base-station linearity requirement.

A photograph of the experimental setup for the fabricated feedforward amplifier configuration is illustrated in Fig. 19. As discussed earlier, an error-signal injection coupler was directly connected to the coupler at the MPA output, without any delay element at the output of the MPA. In product form, all of the active circuits could be integrated into one module, including the NGD circuit, the vector modulator, the subtractor, the BPF, and the EPA, thereby reducing the size of the whole feedforward system.

V. CONCLUSION

We introduced an alternative topology for feedforward amplifiers that yields substantial efficiency enhancement and size reduction by employing a DE NGD circuit. We discussed the design procedure and considerations for the DE NGD circuit. With the fabricated two-stage DE NGD circuit with a 30-MHz

bandwidth for a WCDMA downlink band, the feedforward amplifier of the proposed topology experimentally achieved the highest efficiency among those previously reported in the literature, with additional advantages as to size and cost reduction.

Among the various linearization techniques used for a base-station transmitter, although old-fashioned, the feedforward method still has many advantages over DPD techniques, including all RF linearization and immunity to long-term memory effects. The proposed topology is thought to be especially suitable for a system with a lower frequency of operation, where the physical size of the delay element is relatively large for the system. In addition, when this technique is applied to high-power systems with a few kilowatts, additional efficiency, size, and cost improvements may be fairly realized.

REFERENCES

- [1] H. S. Black, "Translating System," U.S. Patent 1 686 792, Oct. 29, 1928.
- [2] H. S. Black, "Wave Translation System," U.S. Patent 2 102 671, Dec. 21, 1937.
- [3] H. Seidel, "A microwave feedforward experiment," *Bell Syst. Tech. J.*, vol. 50, pp. 2879–2916, 1971.
- [4] S. C. Cripps, *Advanced Techniques in RF Power Amplifier Design*. Norwood, MA: Artech House, 2002.
- [5] N. Potheary, *Feedforward Linear Power Amplifiers*. Norwood, MA: Artech House, 1999, pp. 125–138.
- [6] P. B. Kenington, *High-Linearity RF Amplifier Design*. Norwood, MA: Artech House, 2000, pp. 251–350.
- [7] Y. K. G. Hau, V. Postoyalko, and J. R. Richardson, "Sensitivity of distortion cancellation in feedforward amplifiers to loops imbalances," in *IEEE MTT-S Int. Microw. Symp. Dig.*, 1997, pp. 1695–1698.
- [8] S. G. Kang, I. K. Lee, and K. S. Yoo, "Analysis and design of feedforward power amplifier," in *IEEE MTT-S Int. Microw. Symp. Dig.*, 1997, pp. 1519–1522.
- [9] K. Konstantinou and D. K. Paul, "Analysis and design of broadband, high efficiency feedforward amplifiers," in *IEEE MTT-S Int. Microw. Symp. Dig.*, 1996, pp. 867–870.
- [10] A. S. Andrenko, K. Horiguchi, M. Nakayama, Y. Ikeda, and O. Ishida, "Optimization analysis of feedforward power amplifier," in *IEEE MTT-S Int. Microw. Symp. Dig.*, 1999, pp. 626–629.
- [11] C. L. Larose and F. M. Ghannouchi, "Optimization of feedforward amplifier power efficiency on the basis of drive statistics," *IEEE Trans. Microw. Theory Tech.*, vol. 51, no. 1, pp. 41–54, Jan. 2003.
- [12] C. L. Larose and F. M. Ghannouchi, "Optimal adaptation methods and class of operation: Keys to improving feedforward amplifier power efficiency," *IEEE Trans. Veh. Technol.*, vol. 54, no. 2, pp. 456–467, Mar. 2005.
- [13] S. Rummery and G. R. Branner, "Power amplifier design using feedforward linearization," in *IEEE MTT-S Int. Microw. Symp. Dig.*, 1997, pp. 545–548.
- [14] Y. C. Jeong, D. Ahn, C. D. Kim, and I. S. Chang, "Feedforward amplifier using equal group-delay signal canceller," in *IEEE MTT-S Int. Microw. Symp. Dig.*, 2006, pp. 1530–1533.
- [15] Y. K. G. Hau, V. Postoyalko, and J. R. Richardson, "Design and characterization of a microwave feed-forward amplifier with improved wide-band distortion cancellation," *IEEE Trans. Microw. Theory Tech.*, vol. 49, no. 1, pp. 200–203, Jan. 2001.
- [16] R. N. Braithwaite, "Positive feedback pilot system for second loop control in a feedforward power amplifier," *IEEE Trans. Microw. Theory Tech.*, vol. 55, no. 11, pp. 3293–3305, Nov. 2008.
- [17] H. Choi, Y. Jeong, J. S. Kenney, and C. D. Kim, "Dual-band feedforward linear power amplifier for digital cellular and IMT-2000 base-station," *Microw. Opt. Technol. Lett.*, vol. 51, no. 4, pp. 922–926, Apr. 2009.
- [18] H. Choi, Y. Jeong, J. S. Kenney, and C. D. Kim, "Cross cancellation technique employing an error amplifier," *IEEE Microw. Wireless Compon. Lett.*, vol. 18, no. 7, pp. 488–490, Jul. 2008.
- [19] D. Solli and R. Y. Chiao, "Superluminal effects and negative delays in electronics, and their applications," *Phys. Rev. E, Stat. Phys. Plasmas Fluids Relat. Interdiscip. Top.*, no. 5, pp. 056601 1–0566101 4, Nov. 2002.
- [20] L. Brillouin and A. Sommerfeld, *Wave Propagation and Group Velocity*. New York: Academic, 1960, pp. 113–137.
- [21] S. Lucyszyn, I. D. Robertson, and A. H. Aghvami, "Negative group delay synthesiser," *Electron. Lett.*, vol. 29, no. 9, pp. 798–800, Apr. 1993.
- [22] L. J. Wang, A. Kuzmich, and A. Dogariu, "Gain-assisted superluminal light propagation," *Nature*, vol. 406, no. 6793, pp. 277–279, Jun. 2000.
- [23] M. Kitano, T. Nakanishi, and K. Sugiyama, "Negative group delay and superluminal propagation: An electronic circuit approach," *IEEE J. Sel. Top. Quantum Electron.*, vol. 9, no. 1, pp. 43–51, Jan. 2003.
- [24] B. Ravelo, A. Perennec, and M. Le Roy, "Synthesis of broadband negative group delay active circuits," in *IEEE MTT-S Int. Microw. Symp. Dig.*, Jun. 2007, pp. 2177–2180.
- [25] B. Ravelo, A. Perennec, M. Le Roy, and Y. Boucher, "Active microwave circuit with negative group delay," *IEEE Microw. Wireless Compon. Lett.*, vol. 17, no. 12, pp. 861–863, Dec. 2007.
- [26] B. Ravelo, A. Perennec, and M. Le Roy, "Negative group delay active topologies respectively dedicated to microwave frequencies and base-band signals," *J. EuMA*, vol. 4, pp. 124–130, Jun. 2008.
- [27] B. Ravelo, M. Le Roy, and A. Perennec, "Application of negative group delay active circuits to the design of broadband and constant phase shifters," *Microw. Opt. Technol. Lett.*, vol. 50, no. 12, pp. 3078–3080, Dec. 2008.
- [28] H. Noto, K. Yamauchi, M. Nakayama, and Y. Isota, "Negative group delay circuit for feed-forward amplifier," in *IEEE MTT-S Int. Microw. Symp. Dig.*, Jun. 2007, pp. 1103–1106.
- [29] H. Choi, K. Song, C. D. Kim, and Y. Jeong, "Synthesis of negative group delay time circuit," in *Asia-Pacific Microw. Conf. Dig.*, 2008, p. B5-08.
- [30] H. Choi, Y. Kim, Y. Jeong, and C. D. Kim, "Synthesis of reflection type negative group delay circuit using transmission line resonator," in *Proc. 39th Eur. Microw. Conf.*, Sep. 2009, pp. 902–905.
- [31] G. Matthaei, L. Young, and E. M. T. Jones, *Microwave Filters, Impedance-Matching Networks, and Coupling Structures*. Dedham, MA: Artech House, 1980.
- [32] T. Ogawa, T. Iwasaki, H. Maruyama, K. Horiguchi, M. Nakayama, Y. Ikeda, and H. Kurebayashi, "High efficiency feed-forward amplifier using RF predistortion linearizer and the modified doherty amplifier," in *IEEE MTT-S Int. Microw. Symp. Dig.*, 2004, pp. 537–540.
- [33] J. Yoon and C. Seo, "Improvement of broadband feedforward amplifier using photonic bandgap," *IEEE Microw. Wireless Compon. Lett.*, vol. 11, no. 11, Nov. 2001.
- [34] K. J. Parsons and P. B. Kenington, "The efficiency of a feedforward amplifier with delay loss," *IEEE Trans. Veh. Technol.*, vol. 43, no. 2, pp. 407–412, May 1994.
- [35] K. J. Parsons and P. B. Kenington, "Effect of delay mismatch on a feedforward amplifier," *Proc. Inst. Elect. Eng.—Circuits Devices Syst.*, vol. 141, no. 2, pp. 140–144, Apr. 1994.
- [36] K. Horiguchi, M. Nakayama, Y. Sakai, K. Totani, H. Senda, Y. Ikeda, and O. Ishida, "A high efficiency feedforward amplifier with a series diode linearizer for cellular base stations," in *IEEE MTT-S Int. Microw. Symp. Dig.*, 2001, pp. 797–800.



Heungjae Choi (S'06) received the B.S. and M.S. degrees in electronics and information engineering from Chonbuk National University, Jeonju, Korea, in 2004 and 2006, respectively, and is currently working toward the Ph.D. degree at Chonbuk National University. His master's research focused on the design of dual-band linear PAs for base-station applications.

His research interests include broadband linearization and high-efficiency RF PAs and, recently, negative group delay and its RF and electronic circuit applications.



Yongchae Jeong (M'99) received the B.S., M.S., and Ph.D. degrees from Sogang University, Seoul, Korea, in 1989, 1991, and 1996, respectively, all in electronic engineering.

From 1991 to 1998, he was a Senior Engineer with the Information and Communication Division, Samsung Electronics. Since 1998, he has been with the Division of Electronics and Information Engineering and a chair of the Integrated Circuit Design Education Center (IDEC) Working Group, Chonbuk National University, Jeonju, Korea, where he is currently

a Professor. He currently conducts research in the areas of microwave devices, base-station amplifiers, linearizing technology, and RF integrated circuit design.

Prof. Jeong is a member of the Korea Institute of Electromagnetic Engineering and Science (KIEES).



Chul Dong Kim (M'78) received the B.S. degree in electronic engineering from Seoul National University, Seoul, Korea, in 1971, and the Ph.D. degree from the University of Wisconsin–Madison, in 1985.

Dr. Kim is the President and Chief Executive Office (CEO) of Sewon Teletech Inc., Kyungki, Korea, a company that specializes in RF PAs.



J. Stevenson Kenney (F'08) was born in St. Louis, MO, in 1962. He received the B.S.E.E., M.S.E.E., and Ph.D. degrees from the Georgia Institute of Technology, Atlanta, in 1985, 1990, and 1994, respectively, all in electrical engineering.

He has over 14 years of industrial experience in wireless communications. He has held engineering and management positions with Electromagnetic Sciences, Scientific Atlanta, Pacific Monolithics, and Spectrian. In January 2000, he returned to the Georgia Institute of Technology, as an Associate

Professor with the Department of Electrical and Computer Engineering. He has authored or coauthored more than 100 technical papers, book chapters, and conference presentations in the areas of acoustics, microsystems, and microwave design.

Dr. Kenney is an elected member of the IEEE Microwave Theory and Techniques Society (MTT-S) Administrative Committee and served as its president in 2007.